

EFFECTS OF CAVITATION ON ROTORDYNAMIC FORCE MATRICES

C.E. Brennen, R. Franz and N. Arndt
California Institute of Technology
Pasadena, CA 91125

ABSTRACT

When designing a turbomachine, particularly one which is to operate at high speed, it is important to be able to predict the fluid-induced forces, both steady and unsteady, acting on the various components of the machine. This paper concentrates on the fluid-induced rotordynamic forces acting upon the impeller and therefore on the bearings. Self-excited whirl, where the rotor moves away from and whirls along a trajectory eccentric to its undeflected position, can result from these fluid-induced forces. The purpose of the present work is to study the full range of these forces so that they can be included in any rotordynamic analysis at the design stage.

To study the fluid-induced rotordynamic force on an impeller vibrating around its machine axis of rotation, an experiment in forced vibration was conducted. The prescribed whirl trajectory of the rotor is a circular orbit of a fixed radius. A rotating dynamometer mounted behind the rotor measures the force on the impeller. The force measured is a combination of a steady radial force due to volute asymmetries and an unsteady force due to the eccentric motion of the rotor. These measurements have been conducted over a full range of whirl/impeller speed ratios and different flow coefficients for various turbomachines including both centrifugal impellers and axial inducers. A destabilizing force was observed over a region of positive whirl ratio. The range of flow conditions includes an examination of the effects of cavitation on the observed rotordynamic forces.

NOMENCLATURE

[A]	hydrodynamic force matrix, non-dimensionalized by $\frac{1}{2}\rho u_2^2 A_F / r_2$
A_1, A_2	impeller inlet area (πr_1^2), impeller outlet area ($2\pi r_2 b_2$) or inducer largest cross section πr_t^2
A_F	area used to non-dimensionalize forces, impeller: A_2 , inducer: $2\pi r_t l$
b_2	impeller discharge width
F	6-component generalized force vector, or instantaneous lateral force on the impeller
F_1, F_2	components of the instantaneous lateral force on the impeller in the rotating dynamometer reference frame
F_x, F_y	components of the instantaneous lateral force on the impeller in the stationary volute frame (X,Y), non-dimensionalized by $\frac{1}{2}\rho u_2^2 A_F$
F_{ox}, F_{oy}	values of F_x and F_y if the impeller was located at the origin of the stationary volute frame, non-dimensionalized by $\frac{1}{2}\rho u_2^2 A_F$
F_n, F_t	components of the lateral force on the impeller which are normal to and tangential to the whirl orbit, averaged over the orbit, non-dimensionalized by $\frac{1}{2}\rho u_2^2 A_F \frac{r}{r_2}$
I/J	ratio of whirl/impeller shaft speeds
l	axial length of the inducer blade at the tip
p_1, p_{t1}	upstream static, total pressure
p_2, p_{t2}	downstream static, total pressure
p_I	static pressure at impeller inlet, $p_{t1} - \frac{1}{2}\rho\left(\frac{Q}{A_1}\right)^2$

p_v	vapor pressure of water
Q	flow rate
r_1, r_2	impeller inlet radius, discharge radius
r_t	inducer tip radius
t	time
u_1	tip speed at impeller inlet, ωr_1
u_2	tip speed at impeller discharge, ωr_2 , or at inducer tip, ωr_t
(X,Y)	stationary volute reference frame
x,y	instantaneous coordinates of the impeller center in the stationary volute frame (X,Y), non-dimensionalized by r_2 (impeller) or r_t (inducer)
ε	radius of circular whirl orbit (.0495 inch)
θ	angular position of the impeller on the whirl orbit, measured from the volute tongue in the direction of impeller rotation
ρ	density of water
σ	cavitation number, $\frac{p_l - p_v}{\frac{1}{2} \rho u_1^2}$
ϕ	flow coefficient, $\frac{Q}{u_2 A_2}$
ψ	total head coefficient, $\frac{p_{t2} - p_{t1}}{\rho u_2^2}$
ω	radian frequency of the impeller (shaft) rotation
Ω	radian frequency of the whirl motion $= I\omega/J$
HPOTP	High Pressure Oxygen Turbopump
LPOTP	Low Pressure Oxidizer Turbopump
SSME	Space Shuttle Main Engine

INTRODUCTION

The force experienced by a rotating turbomachine has an unsteady component related to the lateral vibration of the rotor. Knowledge of the unsteady force is crucial to understanding the rotordynamics of the turbomachine. This force has been measured on pump impellers by various authors: Bolleter et al. (1985), Ohashi & Shoji (1987), Ohashi et al. (1986), Jery et al (1985), and Jery (1987). Bolleter translated the impeller inside a vaned diffuser along a single axis using a "rocking arm" excited by a transient frequency sweep. The test section was typical of a single stage of a boiler feed pump. Ohashi, using a circular whirl motion, first tested two-dimensional impellers and then employed a rebuilt eccentric whirl mechanism to test a centrifugal impeller in a vaned diffuser. This paper presents data taken using the same facility as Jery who had measured the forces on a five bladed centrifugal impeller (designated Impeller X) in various vaneless and vaned diffusers, among them a spiral volute (Volute A). Adkins (1985) and Adkins & Brennen (1988) observed that the pressure distribution around the front shroud of Impeller X had a significant contribution to the hydrodynamic stiffness. He also reported measurements taken with the annular region surrounding the shroud exposed to the housing reservoir. This data was compared with measurements taken without the enlarged annular region surrounding the shroud and with a two dimensional model of the impeller, Franz et al. (1987), demonstrating that the large shroud clearances reduce the magnitude of the rotordynamic forces for reverse whirl and destabilizing forward whirl, whirl ratios less than the zero crossing whirl ratio of the average tangential force. Bolleter, who had a smaller gap between the impeller shroud and the casing, measured larger forces. The results presented in this paper indicate the dependence of the rotordynamic forces upon whirl ratio for various turbomachines: the centrifugal Impeller X, an axial inducer and one half of the double-suction impeller of the HPOTP (High Pressure Oxygen Turbopump) of the SSME (Space Shuttle Main Engine). The operating region of the centrifugal impeller has been extended to include the effect of cavitation.

EXPERIMENTAL FACILITY

The references (Jery et al. 1985 and Jery 1987) provide a description of the facility, a water recirculating pump loop, closed to the atmosphere. By altering the absolute pressure of air inside an air bladder in the reservoir, the datum pressure of the entire loop can be controlled which enables tests in the presence of cavitation. The dynamometer, composed of two parallel plates connected by four strain-gaged posts, is mounted between the impeller and the drive shaft. It measures the six components of a generalized force vector \mathbf{F} acting on the impeller. The impeller is made to whirl in a circular orbit eccentric to the volute center of radius $\epsilon = .0495$ inch, in addition to the normal shaft rotation, using a double bearing cartridge assembly. Figure 1 shows the test section and the eccentric drive mechanism. The face seal on the back shroud of the impeller has been removed (part #16 of Fig. 1) and its fixture machined out to open up the region behind the impeller around the dynamometer, (Jery 1985, 1987), thus reducing the parasitic hydrodynamic forces acting on the external surfaces of the submerged dynamometer. Since the eccentric motion is in the lateral plane, perpendicular to the impeller centerline, only the two components of the force vector \mathbf{F} in this lateral plane will be discussed.

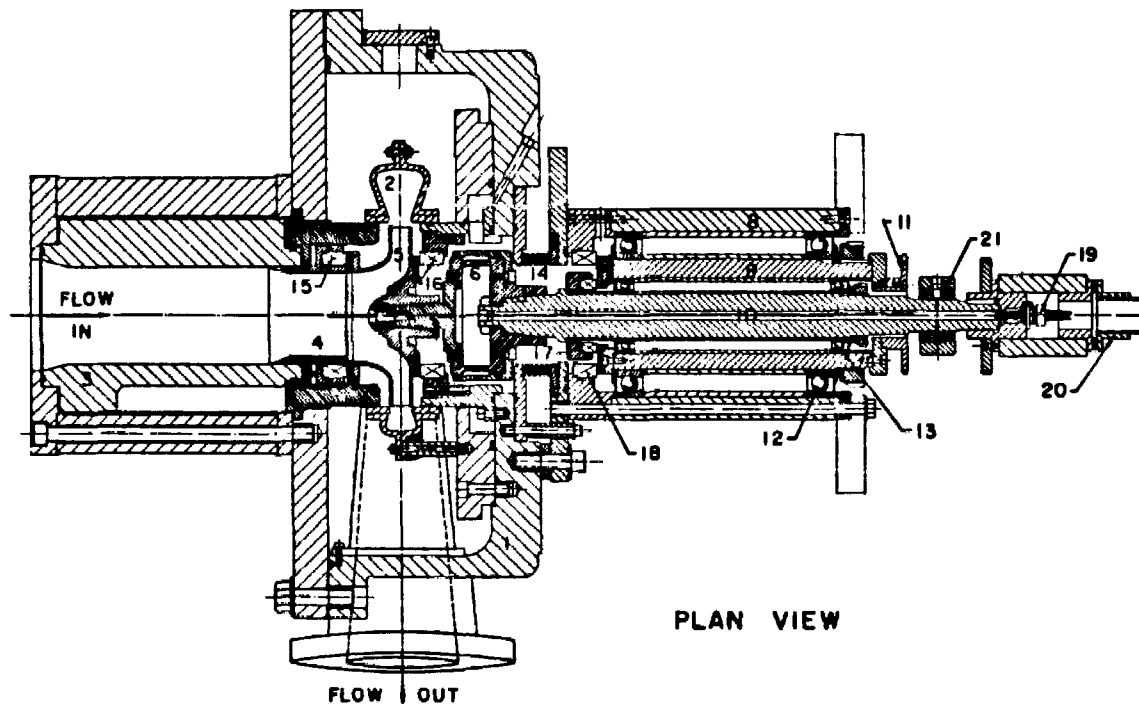
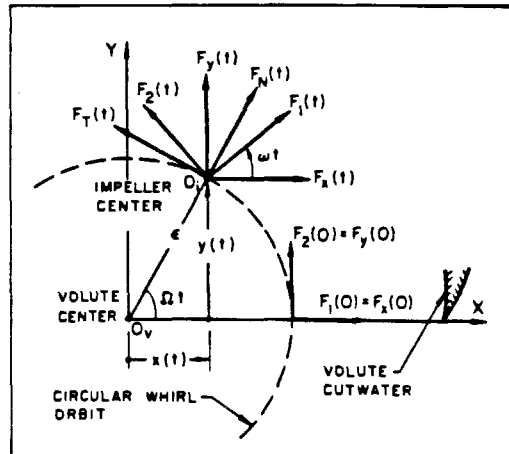


Figure 1. Assembly drawing of the test section and the eccentric drive mechanism. Pump housing, (1); volute (2); inlet connection (3); inlet bell (4); impeller (5); rotating dynamometer (6); eccentric drive mechanism: outer and inner bearing carriers (8 and 9), main shaft (10), orbiting motion sprocket (11); outer and inner bearing sets (12 and 13); bellows (14); impeller front and back (removed) face seals (15 and 16); eccentric drive inner and outer face seals (17 and 18); strain gage cable connector (19); flexible coupling (20); and air bearing stator (21).

Figure 2. Schematic representation of the lateral forces on an impeller whirling in a circular orbit. F_1 and F_2 are in the rotating dynamometer frame. F_x and F_y are in the stationary volute frame. F_n and F_t are in the local polar coordinate frame, normal to and tangential to the circular whirl orbit.



Referring to Fig. 2, these forces, in the stationary volute frame of reference, assuming a small displacement, can be represented by

$$\mathbf{F}(t) = \mathbf{F}_0 + [\mathbf{A}(\Omega/\omega)]\epsilon(t)$$

The lateral force, $\mathbf{F}(t)$, can be considered as the sum of two forces: a steady force, \mathbf{F}_0 , which the impeller would experience if located at the volute center, and an unsteady force due to the eccentric motion of the impeller, represented by a force matrix $[\mathbf{A}]$; $\epsilon(t)$ is the displacement vector of the impeller from the volute center. In general the fluid-induced rotordynamic matrix $[\mathbf{A}]$ will be a function not only of the whirl ratio, Ω/ω , but also of the operating conditions of the turbomachine. To obtain $[\mathbf{A}]$ experimentally at a given whirl ratio and operating condition, two experiments are performed. Identical tests are performed in air and in water. The forces from the former experiment are subtracted from the latter in order to extract the fluid-induced forces. This accounts for imbalance forces and gravitational forces. The buoyancy force on the rotor is subtracted separately. The presented steady force is the average of the computed steady force of each whirl ratio test at the same operating condition unless specified otherwise.

Dimensionless quantities are used throughout (see Nomenclature for definitions). The area used in non-dimensionalizing the forces is not the same for the three turbomachines presented. For the impellers the centrifugal discharge area was used, whereas for Inducer VII the cylindrical surface swept out by the inducer blade tip during rotation without whirl was used. The numerical quantities used to non-dimensionalize the results are given in Table 1.

Table 1. Inducer/Impeller Dimensions

Impeller	r_1 (inch)	r_2 (inch)	b_2 (inch)	r_t (inch)	l (inch)	# blades
X	1.954	3.188	.62	-	-	5
Y	1.6	3.19	.65	-	-	6
R	2.425	3.3	.57	2.35	1.475	4/8
Inducer VII	-	-	-	1.993	.95	3

The unsteady force due to the eccentric motion of the impeller can be represented in terms of the forces, F_n and F_t , normal to and tangential to the whirl orbit, averaged over the orbit. The normal force is considered positive outward, the tangential force is considered positive when in the direction of the velocity of the whirl motion. For the imposed circular whirl orbit

$$F_n = \frac{1}{2}(A_{xx} + A_{yy})$$

$$F_t = \frac{1}{2}(-A_{xy} + A_{yx})$$

Whenever the tangential force is in the same direction as the whirl motion it encourages the whirl motion and is thus destabilizing. A positive normal force tends to increase the radius of the whirl motion. Since the rotordynamic matrix $[A]$ should be independent of the rotation of the axes, it follows that $A_{xx} = A_{yy}$ and $A_{xy} = -A_{yx}$. This was confirmed experimentally (Jery 1985, 1987) and therefore the forces F_n and F_t represent all of the necessary rotordynamic information.

EXPERIMENTS AND RESULTS

Data will be presented for the turbomachines tested in the following sequence: Impeller R, one half of the double-suction impeller of the HPOTP of the SSME, in Volute E, Inducer VII, an axial inducer, and the centrifugal Impeller X in Volute A. Unlike previous impellers tested in the facility, Impeller R has an inducer. The behavior of the unsteady forces with whirl ratio were different for Impeller R than for the other centrifugal impellers, such as Impeller X. This suggested that the inducer could be responsible for some interesting rotordynamic effects. Consequently axial inducers, which had been used previously in transfer function tests, were installed in the test section. Data from one of them is presented here. The effect of cavitation on the rotordynamic matrices is also of interest not only for centrifugal impellers but also for inducers. To investigate this the operating conditions of the centrifugal Impeller X were extended to include cavitation.

Impeller R

One half of the double-suction impeller of the HPOTP of the SSME, Impeller R, was installed in Volute E. The impeller has eight blades and an inducer with four blades. Some modifications were made prior to installation. Most importantly the outlet diameter was reduced from 6.85 to 6.60 inch. This was tested with Volute E which has seventeen, circular arc vanes and an elliptical cross section. Fig. 3 is an assembly drawing showing Impeller R installed in Volute E. Front and back face seal clearances were .005 inch. The inducer had a mean clearance of .1 inch. Data were taken with a main shaft speed of 1000 RPM. The non-cavitating performance curve is given in Fig. 4. The best efficiency point for Impeller R in the facility was near $\phi = .11$.

The steady force on Impeller R is presented in Fig. 5. There is a small variation with flow coefficient. F_n and F_t are presented in Fig. 6-7. For $\phi = 0.14$ the curve of F_n has a parabolic shape and F_t can be approximated by a straight line, with a region of destabilizing whirl in the range $0 < \Omega/\omega < 0.2$. For $\phi = 0.09$ F_t is approximately constant for whirl ratios of $-0.1 < \Omega/\omega < 0.4$, while for $\phi = 0.07$ F_t resembles a cubic function. Since F_t crosses the axis three times, there exist regions of stabilizing and destabilizing whirl for $0.0 < \Omega/\omega < 0.6$. At these lower flow coefficients, F_n has departed from a smooth parabola over this whirl ratio range. Franz & Arndt (1986) present the similar data for more flow coefficients, in addition to tests in a vaneless volute and in the housing without a volute. A strong dependence of F_n and F_t upon Ω/ω for low flow coefficients is common to these measurements.

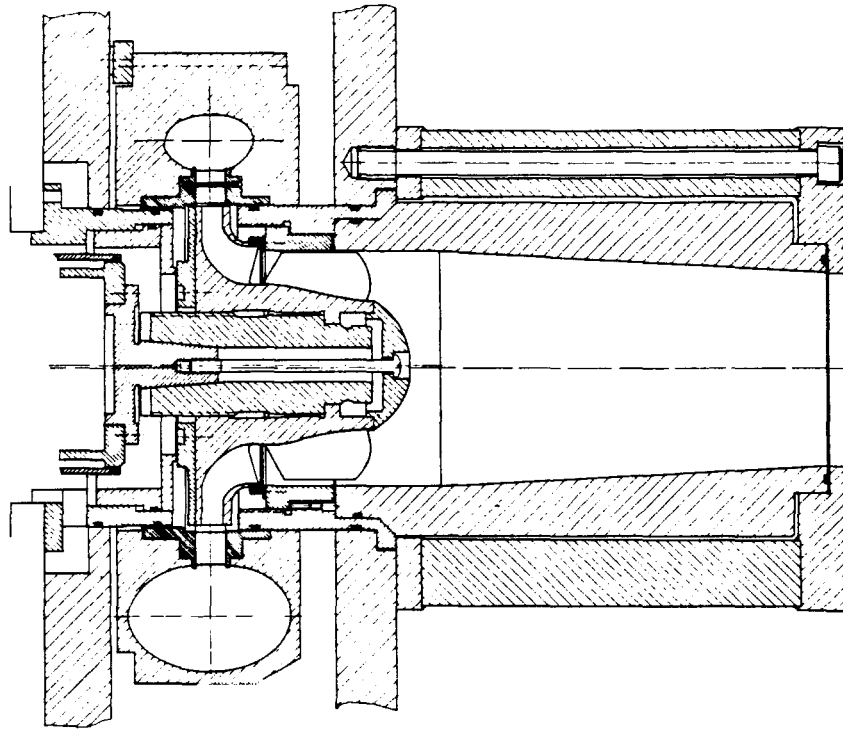


Figure 3. Assembly drawing of Impeller R and Volute E installed in the test section.

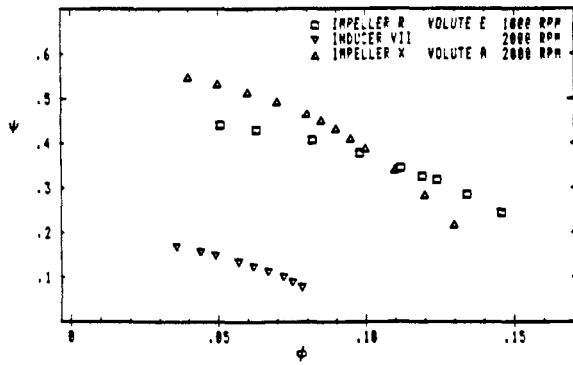


Figure 4. Non-cavitating performance curve of Impeller R in Volute E at 1000 RPM, of Inducer VII at 2000 RPM and of Impeller X in Volute A at 2000 RPM.

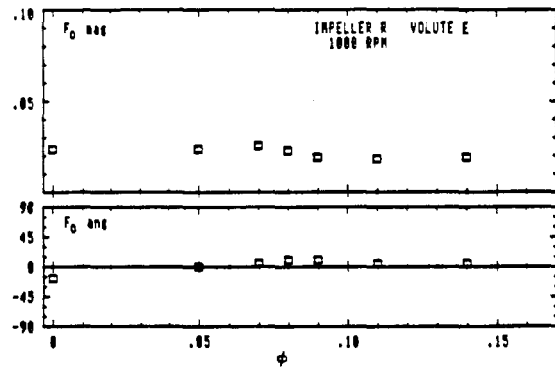


Figure 5. The magnitude and direction of the steady force on Impeller R in Volute E at 1000 RPM as a function of flow coefficient.

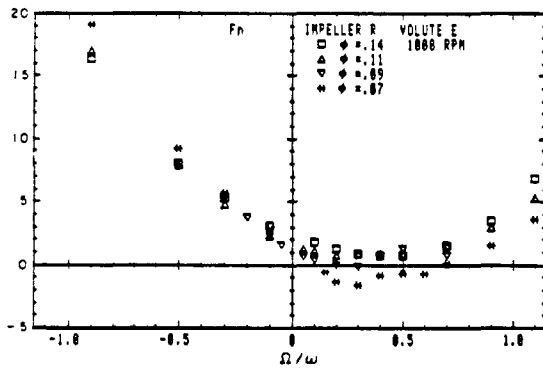


Figure 6. Average normal force on Impeller R in Volute E at 1000 RPM for various flow coefficients.

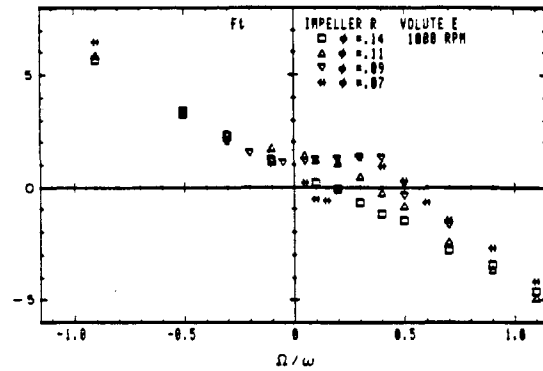


Figure 7. Average tangential force on Impeller R in Volute E at 1000 RPM for various flow coefficients.

Similar changes in the shape of $F_t(\Omega/\omega)$ were observed in earlier tests on the centrifugal Impellers X and Y. These two impellers have similar geometric characteristics and five and six blades, respectively. Previously Jery et al. (1985) and Jery (1987) have reported the changes in $F_t(\Omega/\omega)$ with flow coefficient for Impeller X and Volute E. Tests involving Impeller X and Y showed that at $\phi = .06$, F_t exhibited a cubic behavior in the range of positive destabilizing whirl ratio as shown in Fig. 8. Unlike Impeller R, the curves of F_t for Impellers X and Y cross the axis once. The region $0.0 < \Omega/\omega < 0.5$ is entirely destabilizing. Data had been taken for Impeller X at an even lower flow coefficient, $\phi = .03$. F_t crosses the axis three times, however first under reverse whirl. This behavior did not occur with Impeller X in Volute A, which was designed to be well-matched to Impeller X.

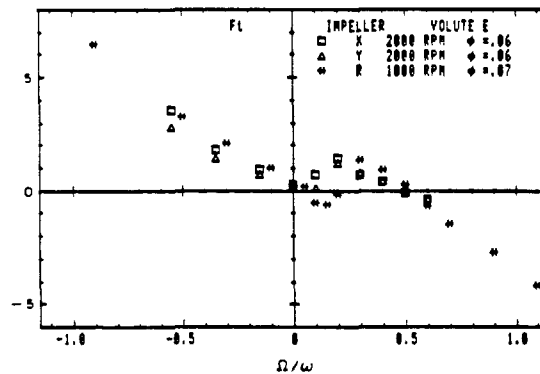


Figure 8. Average tangential force on Impeller X at 2000 RPM, on Impeller Y at 2000 RPM, and on Impeller R at 1000 RPM in Volute E for $\phi = .06$.

Inducer VII

Of the impellers shown in Fig. 8 only Impeller R, which has an inducer, exhibited an F_t which crosses the axis three times, creating a zone of stabilizing whirl ratio bounded by regions of destabilizing whirl ratio for forward whirl. Consequently an axial inducer was installed in the facility to measure the rotordynamic forces upon it, and to find their dependence upon Ω/ω and flow coefficient. The inlet section was modified for the three bladed inducer, Inducer VII, to yield a mean radial clearance of .1 inch, the same clearance as the inducer of Impeller R. An auxiliary pump was used to boost the flow rate through the pump loop for flow coefficients above $\phi = .067$. Fig. 9 shows the inducer installed in the test section. The performance curve is given in Fig. 4, for tests performed with a main shaft speed of 2000 RPM. For $\phi = .067$ the whirl ratio range was extended by rotating the main shaft at 1000 RPM.

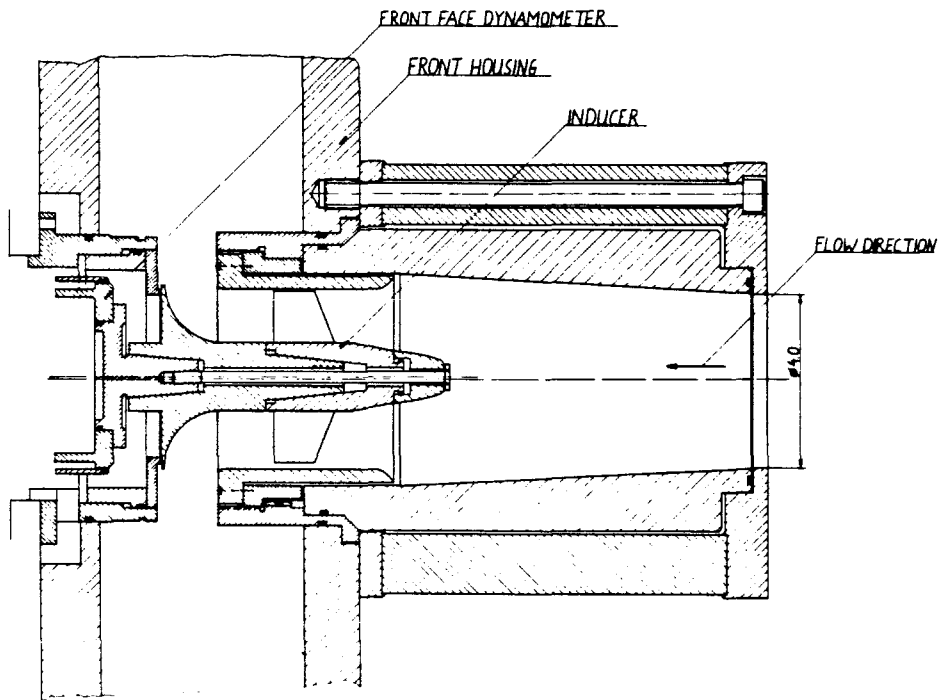


Figure 9. Assembly drawing of Inducer VII installed in the test section.

The steady force is shown in Fig. 10. The magnitude increased with decreasing flow coefficient. The flow leaving the inducer is discharged into the housing which ordinarily contains a volute. The housing itself is essentially a volute and consequently introduces an asymmetry into the flow, which seems to have influenced the steady force on the inducer. Figures 11-12 show F_n and F_t , respectively. At the highest flow coefficient shown, the curve F_n vs Ω/ω resembles a parabola. For lower flow coefficients the parabolic shape is perturbed in the region of low forward whirl. The curve F_t has several zero crossings for low flow coefficients. Also the curvature of F_t changes abruptly in this region. From tufts placed 1 inch upstream of the inducer leading edge, flow reversal was observed at $\phi = .07$.

Figure 10. The magnitude and direction of the steady force on Inducer VII at 2000 RPM as a function of flow coefficient. For $\phi > .067$ an auxiliary pump was used.

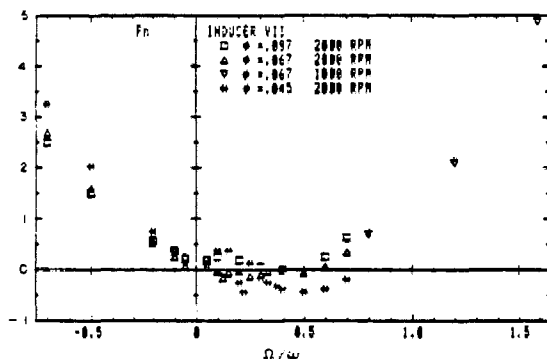
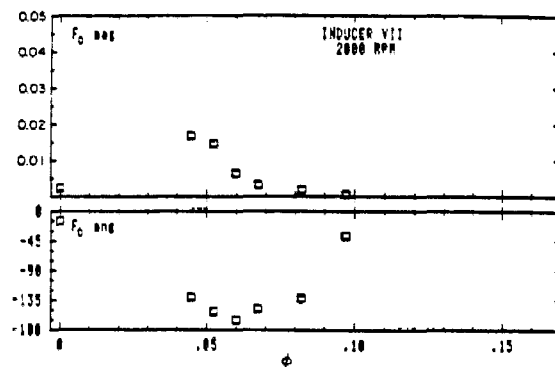


Figure 11. Average normal force on Inducer VII at 2000 RPM for various flow coefficients. For $\phi = .097$ an auxiliary pump was used.

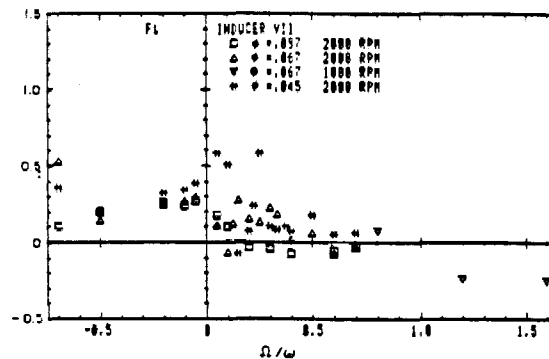


Figure 12. Average tangential force on Inducer VII at 2000 RPM for various flow coefficients. For $\phi = .097$ an auxiliary pump was used.

Arndt & Franz (1986) discuss results for other inducers with the same rather large mean radial clearance of .1 inch for a 4 inch diameter inducer. The four-bladed Inducer VIII, which had the same hub and tip radius at the exit as Inducer VII, also exhibited multiple zero crossings of F_t at low flow coefficients. A scale model of the Low Pressure Oxidizer Turbopump (LPOTP) of the SSME, with four helical blades with a long chord length, followed by a row of twelve short blades, was tested. The flow passage converges until the exit where the hub radius is a significant fraction of the tip radius. Consequently the mean .1 inch tip clearance gap is larger relative to the flow passage cross-section at the inducer exit than the other two inducers. The tangential force was not monotonic with whirl ratio, but it did not have multiple zero crossings. Inducer geometry obviously affects the character of the rotordynamic forces. Inducers VII and VIII, which of the inducers tested most resemble the inducer of Impeller R, had multiple zero crossings in F_t .

Impeller X

The effect of cavitation upon the forces experienced by a whirling centrifugal impeller were examined by installing Impeller X in the test section inside the spiral Volute A. To reduce leakage flow from the impeller exit to the inlet, rings were installed inside the volute, Fig. 13, in addition to the front face seal. The rings at the impeller exit provided a restriction to the flow entering the large

gap surrounding the shroud of the eccentric impeller. These rings were first installed by Adkins (1985, 1988) who had taken pressure measurements circumferentially around the volute entrance and in the annular region surrounding the shroud with the impeller at fixed positions on its whirl orbit. With the rings in place the pressure distribution was more sinusoidal. Their presence would permit a simpler model of the flow geometry in any theoretical work. The front and back rings had an axial clearance of .010 and .005 inch, respectively. The front face seal clearance was .005 inch. Main shaft speed was 2000 RPM. The water had a temperature near 120°F and a dissolved air content of 4 ppm. The results presented were taken at design flow, where the magnitude of the steady force F_o has a minimum.

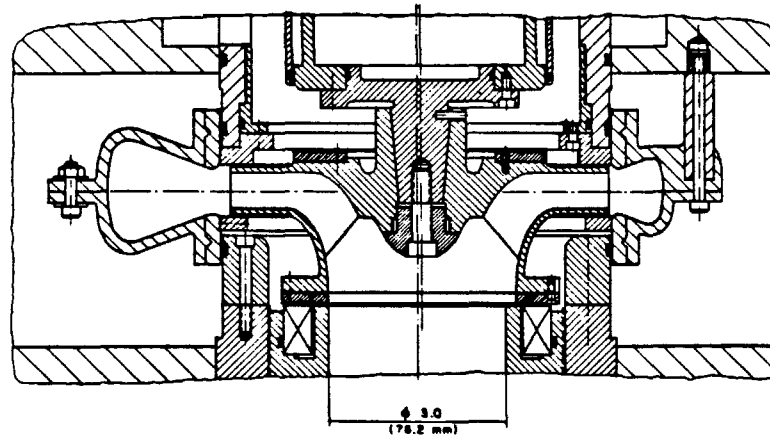


Figure 13. Assembly drawing of Impeller X and Volute A installed in the test section.

The non-cavitating and cavitation performance curves are given in Fig. 4 and Fig. 14, respectively, with $\Omega/\omega = 1$. The last breakdown point of Fig. 14 corresponds to a head loss of 19%, compared to the head rise across the pump at the non-cavitating operating point ($\sigma = 4.37$) where data was taken over a range of whirl ratios. The average normal force, F_n , and tangential force, F_t , as a function of whirl ratio is plotted in Fig. 15 for flow without cavitation and with 3% head loss. At 3% head loss, F_n is slightly smaller and the magnitude of F_t is smaller for positive Ω/ω . The range of destabilizing whirl ratio is not altered by cavitation at 3% head loss.

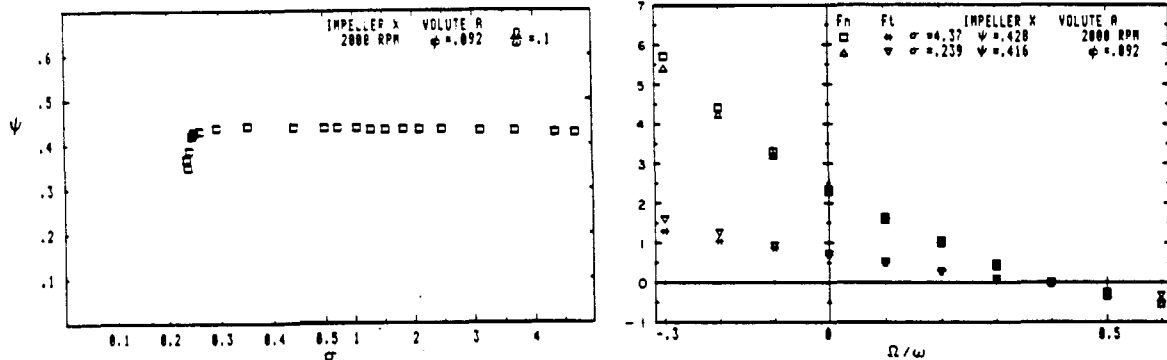


Figure 14. Cavitation performance curve for Impeller X in Volute A at 2000 RPM with $\Omega/\omega = .1$ at design flow ($\phi = .092$).

Figure 15. The average normal and tangential force on Impeller X in Volute A at 2000 RPM at design flow ($\phi = .092$) as a function of whirl ratio for flow without cavitation and with a head loss of 3%.

Using a fixed whirl ratio of $\Omega/\omega = .1$, the effect of cavitation through breakdown on the magnitude and direction of the steady force is plotted against cavitation number in Fig. 16. The magnitude of F_o decreases with decreasing σ until breakdown, where it increases above its non-cavitating value. The direction of F_o rotates away from the tongue in the direction of impeller shaft rotation.

The average normal and tangential force through breakdown for two whirl ratios ($\Omega/\omega = .1$ and $.3$) is given in Fig. 17-18. For $\Omega/\omega = .1$ F_n and F_t decrease with breakdown, however for a head loss greater than 10% there is a slight rise in F_t . $\Omega/\omega = .3$ exhibits similar behavior except in the region between the peak in head rise and 1% head loss, where F_n goes through a trough and F_t a peak. Here the unsteady force increases slightly in magnitude and rotates in a direction to increase the destabilizing tangential force. Figure 19 shows that this perturbation is reflected in the steady force calculated from the $\Omega/\omega = .3$ data, which contradicts the assumption that F_o is independent of whirl ratio. Data taken at flow coefficients below design ($\phi = .060$) and above design ($\phi = .120$) do not show this peculiarity (Franz 1988).

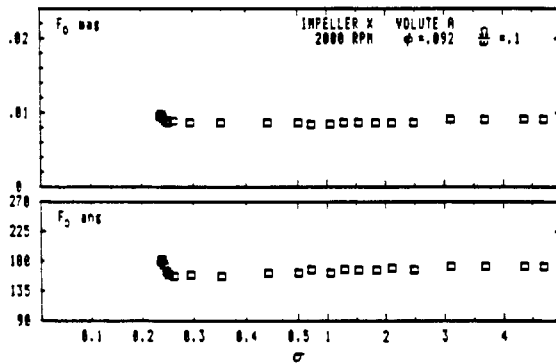


Figure 16. The magnitude and direction of the steady force on Impeller X in Volute A at 2000 RPM with $\Omega/\omega = .1$ at design flow ($\phi = .092$) as a function of the cavitation number.

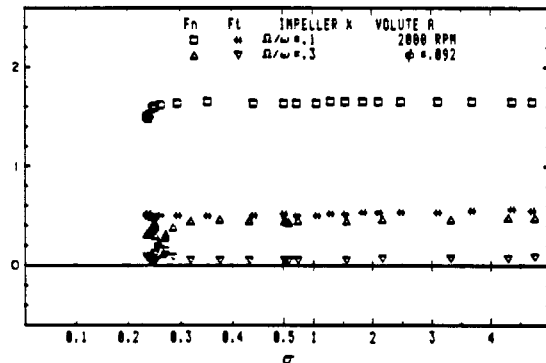


Figure 17. The average normal and tangential force on Impeller X in Volute A at 2000 RPM with $\Omega/\omega = .1$ and $.3$ at design flow ($\phi = .092$) as a function of cavitation number.

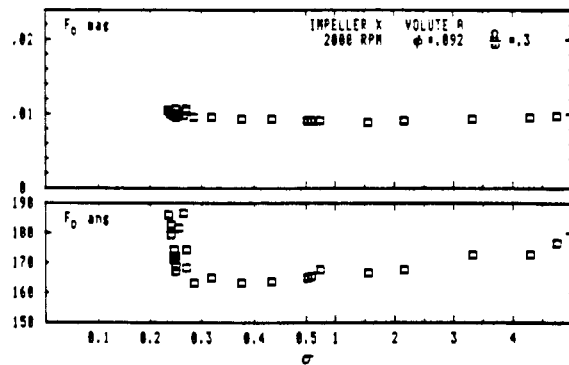


Figure 19. The magnitude and direction of the steady force on Impeller X in Volute A at 2000 RPM with $\Omega/\omega = .3$ at design flow ($\phi = .092$) as a function of the cavitation number.

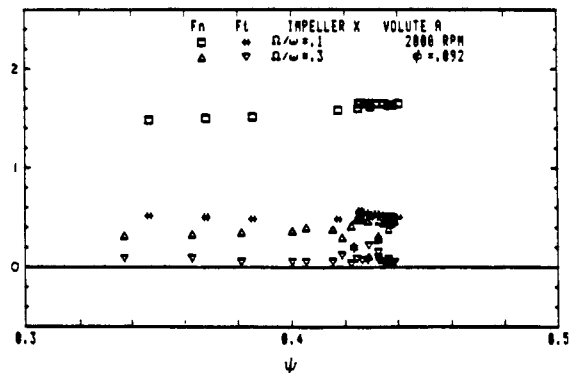


Figure 18. The average normal and tangential force on Impeller X in Volute A at 2000 RPM with $\Omega/\omega = .1$ and $.3$ at design flow ($\phi = .092$) as a function of head coefficient.

CONCLUSION

The rotordynamic forces experienced by a turbomachine depend upon whirl ratio, flow coefficient and also the volute used. Measurements employing a forced vibration experiment have been made on various turbomachines: centrifugal impellers, axial inducers, and a centrifugal impeller with an inducer. Volute used include a spiral volute, a seventeen, circular arc vaned diffuser and the volute housing chamber itself. Typically there is a region of forward whirl for which the average tangential force, F_t , is destabilizing. At low flow coefficients, the tangential force on the impeller, depending upon the volute used, may become a strong function of Ω/ω , to the extent that the region of destabilizing forward whirl may become disjoint, eg. F_t resemble a cubic. It has even been observed that at sufficiently low flow coefficients (for a centrifugal impeller in the seventeen vaned diffuser) a region of reverse whirl had become destabilizing. For the HPOTP, (a centrifugal impeller with an inducer), the appearance of the cubic at low flow coefficients was independent of volute. The occurrence of flow reversal appears to coincide with this transition in the curve of F_t .

A centrifugal impeller was tested at design in the presence of cavitation. The magnitude of F_o varied less than 10% from flow without cavitation to 19% head loss, though its direction rotated. At 3% head loss the destabilizing unsteady forces had decreased slightly. Between peak head rise and 1% head loss for $\Omega/\omega = .3$ there was a perturbation in the unsteady and the steady forces. Passing through the knee of the performance curve, the unsteady force rotated in a direction to increase the destabilizing tangential force, then rotated back. The swing in the steady force vector was first in the direction of impeller rotation. This perturbation contradicts the assumption that F_o is independent of whirl ratio.

ACKNOWLEDGEMENTS

The authors are indebted to the NASA George Marshall Space Flight Center, for continued sponsorship of this research under contract NAS8-33108. The authors want to thank Dr. Acosta and Dr. Caughey for their participation in this research.

REFERENCES

- Adkins, D.R., Brennen, C.E. "Analysis of Hydrodynamic Radial Forces on Centrifugal Pump Impellers," *ASME Journal of Fluids Engineering* Vol. 110, No. 1, 1988, pp 20-28.
- Adkins, D.R., "Analysis of Hydrodynamic Forces on Centrifugal Pump Impellers," Ph.D. Thesis, Division of Engineering and Applied Science, California Institute of Technology, 1985.
- Arndt, N. and Franz, R., "Observations of Hydrodynamic Forces on Several Inducers including the SSME LPOTP," Division of Engineering and Applied Science, California Institute of Technology, 1986, Report No. 249.3.
- Bolleter, U., Wyss, A., Welte, I., and Stürchler, R., "Measurement of Hydrodynamic Interaction Matrices of Boiler Feed Pump Impellers," ASME 85-DET-148.
- Franz, R., "Experimental Investigation of the Effect of Cavitation on the Rotordynamic Forces on a Whirling Centrifugal Pump Impeller," Ph.D. Thesis, Division of Engineering and Applied Science, California Institute of Technology, 1988, in preparation.

Franz, R., Arndt, N., Caughey, T.K., Brennen, C.E., and Acosta, A.J., "Rotordynamic Forces on Centrifugal Pump Impellers," Eighth Conference of Fluid Machinery, Budapest, Hungary, September 15-18, 1987.

Franz, R., and Arndt, N., "Measurements of Hydrodynamic Forces on the Impeller of the HPOTP of the SSME," Division of Engineering and Applied Science, California Institute of Technology, 1986, Report No. 249.2.

Jery, B., "Experimental Study of Unsteady Hydrodynamic Force Matrices on Whirling Centrifugal Pump Impellers," Ph.D. Thesis, Division of Engineering and Applied Science, California Institute of Technology, 1987.

Jery, B., Brennen, C.E., Caughey, T.K., and Acosta, A.J., "Forces on Centrifugal Pump Impellers," "Second International Pump Symposium," Houston, Texas, April 29-May 2, 1985.

Ohashi, H., Shoji, H., "Lateral Fluid Forces on a Whirling Centrifugal Impeller (2nd Report: Experiment in Vaneless Diffuser)," *ASME Journal of Fluids Engineering*, Vol. 109, No. 2, 1987, pp. 100-106.

Ohashi, H., Hatanaka, R., and Sakurai, A., "Fluid Force Testing Machine for Whirling Centrifugal Impeller," International Conference on Rotordynamics, Tokyo, Japan, Sept. 14-17, 1986.